Compressibility of molten Apollo 17 orange glass and implications for density crossovers in the lunar mantle

van Kan, M.; Agee, C.B.; Duncan, M.S.; van Westrenen, W.

published in
Geochimica et Cosmochimica Acta
2011

DOI (link to publisher)
10.1016/j.gca.2010.11.022

document version
Publisher's PDF, also known as Version of record

Available online at www.sciencedirect.com
ScienceDirect
Geochimica et Cosmochimica Acta 75 (2011) 1161–1172
Geochimica et Cosmochimica Acta
www.elsevier.com/locate/gca

Compressibility of molten Apollo 17 orange glass and implications for density crossovers in the lunar mantle

Mirjam van Kan Parker [a,*], Carl B. Agee [b], Megan S. Duncan [b], Wim van Westrenen [a]

[a] Faculty of Earth and Life Sciences, VU University Amsterdam, De Boelelaan 1085, 1081 HV Amsterdam, The Netherlands
[b] Institute of Meteoritics, University of New Mexico, United States

Received 20 September 2010; accepted in revised form 24 November 2010; available online 4 December 2010

Abstract

We performed density measurements on a synthetic equivalent of lunar Apollo 17 74,220 "orange glass", containing 9.1 wt% TiO_2, at superliquidus conditions in the pressure range 0.5–8.5 GPa and temperature range 1723–2223 K using the sink/float technique. In the lunar pressure range, two experiments containing pure forsterite (Fo_{100}) spheres at 1.0 GPa and 1727 K, and at 1.3 GPa–1739 K, showed neutral buoyancies, indicating that the density of molten orange glass was equal to the density of Fo_{100} at these conditions (3.09 ± 0.02 g cm^{-3}). A third tight sink/float bracket using Fo_{90} spheres corresponds to a melt density of 3.25 ± 0.02 g cm^{-3} at ~2.8 GPa and ~1838 K.

Our data predict a density crossover for the molten orange glass composition with equilibrium orthopyroxene at ~2.8 GPa, equivalent to a depth of ~600 km in the lunar mantle, and a density of ~3.25 g cm^{-3}. This crossover depth is close to the orange glass multiple saturation point, representing its minimum formation depth, at the appropriate oxygen fugacity (2.8–2.9 GPa). A density crossover with equilibrium olivine is predicted to fall outside the lunar pressure range (>4.7 GPa), indicating that molten orange glass is always less dense than its equilibrium olivines in the Moon. Our data therefore suggest that that lunar liquids with orange glass composition are buoyant with respect to their source region at $P <$ ~2.8 GPa, enabling their initial rise to the surface without the need for additional external driving forces.

Fitting the density data to a Birch–Murnaghan equation of state at 2173 K leads to an array of acceptable solutions ranging between 16.1 and 20.3 GPa for the isothermal bulk modulus K_{2173} and 3.6–8 for its pressure derivative K', with best-fit values $K_{2173} = 18.8$ GPa and $K' = 4.4$ when assuming a model 1 bar density value of 2.86 g cm^{-3}. When assuming a slightly lower 1 bar density value of 2.84 g cm^{-3} we find a range for K_{2173} of 14.4–18.0 and K' 3.7–8.7, with best-fit values of 17.2 GPa and 4.5, respectively.

1. INTRODUCTION

Lunar mare volcanism produced a diverse array of basalts and volcanic glasses (e.g. Delano, 1986; Shearer et al., 2006). The picritic volcanic glasses are characterised by a broad range in titanium content, with values ranging up to 16.4 wt%. They have relatively high Mg numbers and are thought to represent the most primitive lunar magmas sampled to date (Delano, 1990). Understanding their origin is therefore crucial for understanding lunar magmatic evolution.

Experimentally determined multiple-saturation points for the picritic glasses, which provide estimates for their minimum depths of origin, suggest they were formed at great depths in the lunar interior (250–500 km, equivalent to pressures between 1.2 and 2.5 GPa (e.g. Grove and Krawczynski, 2009). The combination of inferred deep formation and observed high titanium and iron contents begs the question as to whether these picritic melts were more or less dense than their source regions. Delano (1990) first tested the potential role of density inversions between

* Corresponding author. Tel.: +31205983725.
E-mail address: mirjam.van.kan@falw.vu.nl (M. van Kan Parker).

0016-7037/$ - see front matter © 2010 Elsevier Ltd. All rights reserved.
doi:10.1016/j.gca.2010.11.022

molten picritic glass compositions and co-existing equilibrium olivine and orthopyroxene, and found that density inversions (at which melts become denser than co-existing solids) are expected to occur at depths relevant to the generation of picritic lunar glasses. At sufficiently high TiO_2 concentrations, molten lunar glasses could become too dense to reach the surface and would in fact sink deeper within the lunar interior upon formation.

Circone and Agee (1996) tested whether crystal–liquid density inversions in fact played a role during petrogenesis of the picritic glasses by measuring the density of the high titanium end member composition ('Apollo 14 black glass', containing 16.4 wt% TiO_2) at high P and T using the so-called sink/float technique. They identified density crossovers at ~0.5 GPa for equilibrium orthopyroxene and ~2.0 GPa for equilibrium olivine, corresponding to lunar depths of 100 and 410 km, respectively. The multiple saturation point for this black glass composition is ~1.5 GPa (Wagner and Grove, 1997), showing that crystal–liquid density inversions at high P–T conditions could indeed have played an important role during the petrogenesis of these high titanium bearing magmas: the relatively high density of high-titanium lunar basalts should have impeded eruption from their depth of formation e.g. their multiple saturation depth. The fact these lunar liquid compositions did erupt suggests additional factors played a role, such as the presence of small amounts of volatiles (e.g. Elkins-Tanton et al., 2003a; Nicholis and Rutherford, 2009).

Smith and Agee (1997) assessed the importance of crystal–liquid density inversions for the genesis of the low-Ti end-member ('Apollo 15 green C glass' containing 0.23 wt% TiO_2) and predicted a density crossover with orthopyroxene at 3.5 GPa, equivalent to a lunar depth of ~800 km, which is significantly deeper compared to the multiple saturation depth at ~1.3 GPa reported by Elkins-Tanton et al. (2003b). This indicates that molten green glass would be buoyant with respect to its source region, facilitating eruption.

To date however, the density and scope for crystal–liquid density crossovers of the intermediate-high titanium, Apollo 17 74,220 orange glass, have not been determined experimentally. To improve our understanding of the density variations and compressibilities of molten lunar glasses we studied the liquid density of a synthetic equivalent of the Apollo 17 (A17) 74,220 orange glass, containing 9.12 wt% TiO_2. Our experiments cover the P–T range of 0.5–3 GPa, 1723–1853 K, directly relevant to the lunar interior. Additional experiments with P–T ranging between 5.5 and 8.5 GPa and 2123–2223 K were carried out in order to better constrain the compressibility of molten orange glass, and its variation with pressure.

2. EXPERIMENTAL METHODS

2.1. Experimental procedures

To determine the density of molten Apollo 17 (A17) 74,220 orange glass we used the sink/float sphere technique (Agee and Walker, 1988). This method has been successfully used to bracket the high-pressure densities of various silicate liquids (Agee and Walker, 1993; Suzuki et al., 1995; Circone and Agee, 1996; Knoche and Luth, 1996; Smith and Agee, 1997; Agee, 1998, 2008; Suzuki and Ohtani, 2003). The underlying principle of this method is that by using spheres of known density, their sinking (denser) or floating (less dense) ability provides a density bracket of the liquid of interest. In case the spheres do not move they are considered neutrally buoyant, e.g. they are assumed of equal density to the studied material. However, when no movement of the spheres is observed this should only be considered to reflect neutral buoyancy conditions when the experiment is confirmed by preferably both a sink and float experiment at near P–T conditions.

The starting material is a microcrystalline equivalent of the A17 74,220 orange glass composition (Table 1), synthesised and kindly provided by Mike Krawcynzki (MIT, USA). The material was prepared by mixing appropriate amounts of high purity reagent grade powdered oxides and silicates, including Fe_2O_3 in an agate mortar under ethanol for 3 h. Then Fe metal was added and the resulting mixture was ground under ethanol for one additional hour. The powder was fused into a puck using polyvinyl alcohol (DuPont© Elvanol), hung from a 0.10 mm diameter Pt wire and conditioned at a subsolidus temperature of 1323 K in a gas mixing furnace at an oxygen fugacity corresponding to the iron-wüstite buffer for 24 h. The material was quenched in air, crushed and reground in an agate mortar in the absence of fluids for 20 min. Super-liquidus experiments on this material showed that it is close in composition to the natural A17 74,220 orange glass (Table 1; Krawczynski and Grove, 2008).

Sink/float experiments were carried out at the University of New Mexico in a 13 mm Depths of the Earth Quickpress type piston-cylinder (PC) for $P \leqslant 2.5$ GPa, and a Walker type multi-anvil (MA) press for $P > 2.5$ GPa. In the MA set up we used tungsten carbide cubes with a truncation-edge-length (TEL) of 8 mm and octahedral MgO-based pressure media with octahedral-edge-length (OEL) of 14 mm (for more details see Circone and Agee, 1996). T was measured using a Type C ($W_{95}Re_5/W_{74}Re_{26}$) thermocouple for both PC and MA experiments. For the PC experiments the thermocouple was inserted axially below the capsule and for the MA the thermocouple was located on the centre of the outer surface of the Re heater. Phase diagrams for the A17 74,220 orange glass composition by Krawczynski and Grove (2008) were used to estimate appropriate P–T conditions for PC experiments. For MA experiments (at pressures beyond those covered by phase equilibrium studies for this composition) super-liquidus conditions were determined by trial and error.

Two density markers were packed in ~10 mg starting material, one at the bottom and one at the top of a molybdenum capsule (ID 1.6 mm, OD 2.4 mm and 3.7 mm tall including end caps) machined from high-purity rod. Mo capsules were chosen to allow for direct comparison to previous sink/float experiments on molten lunar glasses (Circone and Agee, 1996; Smith and Agee, 1997). The advantages of Mo capsules were previously described in Circone and Agee (1996): (1) They maintain low oxygen fugacity; (2) the large internal dimensions minimise capsule

Table 1
Average Apollo 17 orange glass compositions, compared to black and green glass compositions (Delano, 1986).

	SiO_2	TiO_2	Al_2O_3	Cr_2O_3	FeO	MgO	MnO	CaO	Na_2O	K_2O
wt%										
Apollo 15 green C glass	48.0	0.26	7.74	0.57	16.5	18.2	0.19	8.57	ND	ND
Apollo 17 74,220 orange glass	38.5	9.12	5.79	0.69	22.9	14.9	ND	7.40	0.38	ND
Synthetic starting material, this study*	38.9	8.78	5.81	0.67	22.3	15.7	0.27	7.37	0.26	–
Apollo 14 black glass	34.0	16.4	4.60	0.92	24.5	13.3	0.31	6.90	0.23	0.16

* Data from Krawczynski and Grove (2008).

wall drag effects on moving spheres; (3) thick metal capsules act as heat sinks and their high thermal conductivity promotes a smoother T distribution in MA experiments.

Thermal gradients within the samples are smaller than 20°, based on temperature mapping of PC and MA assemblies comparable to those used here (Watson et al., 2002; van Westrenen et al. 2003). The f_{O_2} in our experiments is close to that of the iron-wüstite buffer (e.g. O'Neill, 1986), which is appropriate for the f_{O_2} conditions in the natural Apollo orange glass (Sato, 1979; Weitz et al., 1997; Nicholis and Rutherford, 2009).

Density markers consisted of synthetic olivine (Fo_{100}), gem quality San Carlos olivine crystals ($Fo_{90}Fa_{10}$) and gem quality pyrope-rich garnets varying in composition from $Py_{56}Al_{28}Gr_{16}$ to $Py_{77}Al_{14}Gr_9$. Density markers were abraded using a Bond air mill (Bond, 1951). The density markers, approximating a spherical shape, varied in diameter between 300 and 600 μm (Circone and Agee, 1996).

Charges were pressurised and subsequently rapidly heated using rates of ~250 K and ~375–400 K per minute for the PC and MA experiments, respectively, and kept at desired P–T conditions for 30 s. In all PC experiments, this duration was sufficient to allow the starting material to fully melt and buoyancy forces to drive the spheres up or down the capsule, while minimizing sample – sphere and sample – capsule interactions. In subsequent higher pressure MA experiments, using garnet density markers, no discernable sphere movement was observed in most of the experiments. To assess whether this was due to slower kinetics of sphere motion at these more extreme conditions, in one experiment ($P = 8.0$ GPa, $T = 2223$ K) we purposely placed a denser sphere at the top and a less dense sphere at the bottom of the charge. In a second experiment ($P = 6.5$ GPa and $T = 2173$ K), designed to investigate the effect of longer experimental duration on sphere movement and Mo contamination, we held the experimental charge at superliquidus conditions for 45 s.

Charges were quenched by switching off the power to the furnace, and then gradually decompressed. Experimental charges were mounted in one inch diameter mounts using Petropoxy, ground using abrasive paper, and polished. The final positions of the marker spheres allowed for a direct determination of relative density.

2.2. Analytical techniques

The run products were embedded in epoxy, polished and carbon coated. The majority of the run products were analysed using a JEOL JXA 8800M electron microprobe at VU University Amsterdam. The accelerating voltage was 15 kV with a beam current of 25 nA. A broad beam of 10 μm diameter was used for glass analyses, and a focused beam for analyses of the mineral density markers. Primary standards include natural olivine and pyrope for the olivine and garnet density markers, respectively, and jadeite (Na), diopside (Mg), corundum (Al), diopside (Si, Ca), fayalite (Fe), orthoclase (K), ilmenite (Ti), Cr_2O_3 (Cr) and tephroite (Mn) for the glass/matrix analysis. A molybdenum standard was used to determine the Mo contents in the glasses. Peak and background count times were 25 and 25 s (2×12.5) for major elements and 36 and 36 s (2×18) for minor elements.

A small number of run products were analysed at the Institute of Meteoritics (IOM), University of New Mexico using a JEOL 8200 electron microprobe, using similar operating conditions and standards. Results from IOM and VU University Amsterdam agree within analytical error (typically approximately 5% relative).

2.3. Density evaluation

To evaluate the density of the mineral spheres we used published equations of state (EOS) parameters for olivine and garnet summarised in Table 2. Sphere densities were calculated using the third order Birch–Murnaghan EOS (Birch, 1947; Angel, 2000):

$$P = \frac{3}{2}K_T\left[\left(\frac{\rho_{T,P}}{\rho_{T,0}}\right)^{7/3} - \left(\frac{\rho_{T,P}}{\rho_{T,0}}\right)^{5/3}\right] \times \left[1 - \frac{3}{4}(4 - K')\left(\left(\frac{\rho_{T,P}}{\rho_{T,0}}\right)^{2/3} - 1\right)\right] \quad (1)$$

in which P is pressure, K_T the isothermal bulk modulus at temperature T, K' its pressure derivative, and $\rho_{T,0}$ and $\rho_{T,P}$ are the densities of the sphere at temperature T and ambient pressure (10^5 Pa) and high pressure, respectively. $\rho_{T,0}$ can be written as:

$$\rho_{T,0} = \rho_{298}(T)\exp\int_{298}^{T}\alpha(T)dT \quad (2)$$

in which the thermal expansion α is defined as:

$$\alpha(T) = \alpha_0 + \alpha_1 T + \alpha_2 T^{-2} \quad (3)$$

Uncertainties associated with using the sink/float technique stem partly from the accuracy and precision of the calibration curves used to constrain sample pressure and temperature conditions, and from the narrowness of the

Table 2
Equation of state parameters for mineral density markers used in this study, assuming linear mixing between end-members.

	K_T (GPa)	dK/dT (GPa/°)	K'	α_0	α_1	α_2	V_0 (Å^3)
Mg_2SiO_4	127.5[a]	−0.02[b]	4.8[a]	3.034E−05	7.422E−09	−5.381E−01[c]	290.1[p]
Fe_2SiO_4	134.6[d]	−0.024[d]	5.2[e]	0.2386E−05	11.53E−09	−0.518E−01[f,g,h]	307.0[g]
$Ca_3Al_2Si_3O_{12}$	165.68[i]	−0.024[j]	5.46[i]	1.951E−05	8.089E−09	−4.972E−01[k]	1659.8[q]
$Mg_3Al_2Si_3O_{12}$	171.32[i]	−0.0258[j]	3.22[i]	2.311E−05	5.956E−09	−4.538E−01[k]	1501.1[q]
$Fe_3Al_2Si_3O_{12}$	185[l]	−0.0268[j]	4.2[l]	1.776E−05	12.14E−09	−5.071E−01[k]	1528.8[q]
$MgSiO_3$	95.8[m]	−0.0274[n]	14.9[m]	2.947E−05	2.694E−09	−0.5588[k]	833.0[m]
$FeSiO_3$	95.1[o]	−0.0237[n]	10.6[o]	2.75E−05[n]			874.2[n]

[a] Jacobs and De Jong (2007).
[b] Liu and Li (2006).
[c] Suzuki (1975).
[d] Graham et al. (1988).
[e] Isaak et al. (1993).
[f] Suzuki et al. (1981).
[g] Smyth (1975).
[h] Hazen (1977).
[i] Conrad et al. (1999).
[j] Sumino and Anderson (1984).
[k] Skinner (1966).
[l] Zhang et al. (1999).
[m] Hugh-Jones and Angel (1994) – valid up to 4 GPa.
[n] Calculated from Hugh-Jones (1997).
[o] Hugh-Jones and Angel (1997).
[p] Hushur et al. (2009).
[q] Chopelas (2006).

sink/float bracket. Based on previous experience with the assemblies used, P and T uncertainties are ±0.1 GPa, ±10 K (PC) and ±0.2 GPa, ±25 K (MA) (see also Circone and Agee, 1995, 1996).

The main uncertainty in the sink/float method is the accuracy of the EOS parameters for the crystal buoyancy markers, in this case olivine and garnet. Literature data show a range of EOS parameters for both olivine and garnet. For the purpose of this study we use the values reported in Table 2. The EOS parameters of natural, multicomponent garnet are less well constrained than for forsteritic olivine (e.g. Geiger, 1999; Lavrentiev et al., 2006). For density calculations we assumed linear relations of elastic properties between the end-members such as pyrope, almandine, and grossular. In addition, the garnet-bearing experiments in this study were performed at temperatures and pressures at which both the thermal expansion and its variation with pressure have not been fully explored. Based on the range of the literature EOS parameters available for olivine, the uncertainty in olivine density calculations at the P–T conditions of this study is calculated to be ±0.02 g cm^{-3}. The uncertainty in garnet density calculations is estimated at twice this number ±0.04 g cm^{-3} to reflect the poorer constraints on EOS parameters, as well as the larger P–T uncertainties in the MA experiments containing garnets compared to the PC experiments containing olivines.

3. RESULTS

Fig. 1a shows representative cross-sections through experimental charges showing floating and sinking density markers. We performed 19 successful experiments in which the synthetic glass was completely molten during the experiment. In ten experiments we used olivine markers, in the other nine garnets were used. The experimental P–T conditions, sink/float results, compositional analyses of the experimental charges and density calculations for all experiments are summarised in Tables 3 and 4. All melts have a quench texture. Quenched melt compositions, as determined by electron microprobe, are consistent between runs, both at low and high pressure (Table 3a and b, respectively). This suggests there was insignificant interaction between the density marker spheres and the orange glass composition starting material during the experiments, consistent with previous work (Circone and Agee, 1996).

The lack of interaction between density markers and starting material was confirmed by mineral sphere spot analyses in each experiment, summarised in Table 4, showing the spheres remained homogeneous in composition during the experiments. Additional electron microprobe line analyses through Fo_{100}, Fo_{90} and garnet ($Py_{70}Al_{18}Gr_{12}$) spheres showed <2% relative standard deviations in major element composition. No reaction rims were visible around any of the olivine spheres (Fig. 1b). Garnet spheres generally did show a ~10 μm thin reaction rim, but the reaction volume is negligible (<0.1 vol%) compared to the volume of melt in all cases (Fig. 1b).

There are minor differences between the experimental glass composition and the starting material (Tables 1 and 3). Mo concentrations are slightly elevated close to the capsule walls, but are fairly homogeneous in the central areas of the samples where the spheres are located. Mo contamination is higher and more variable in the

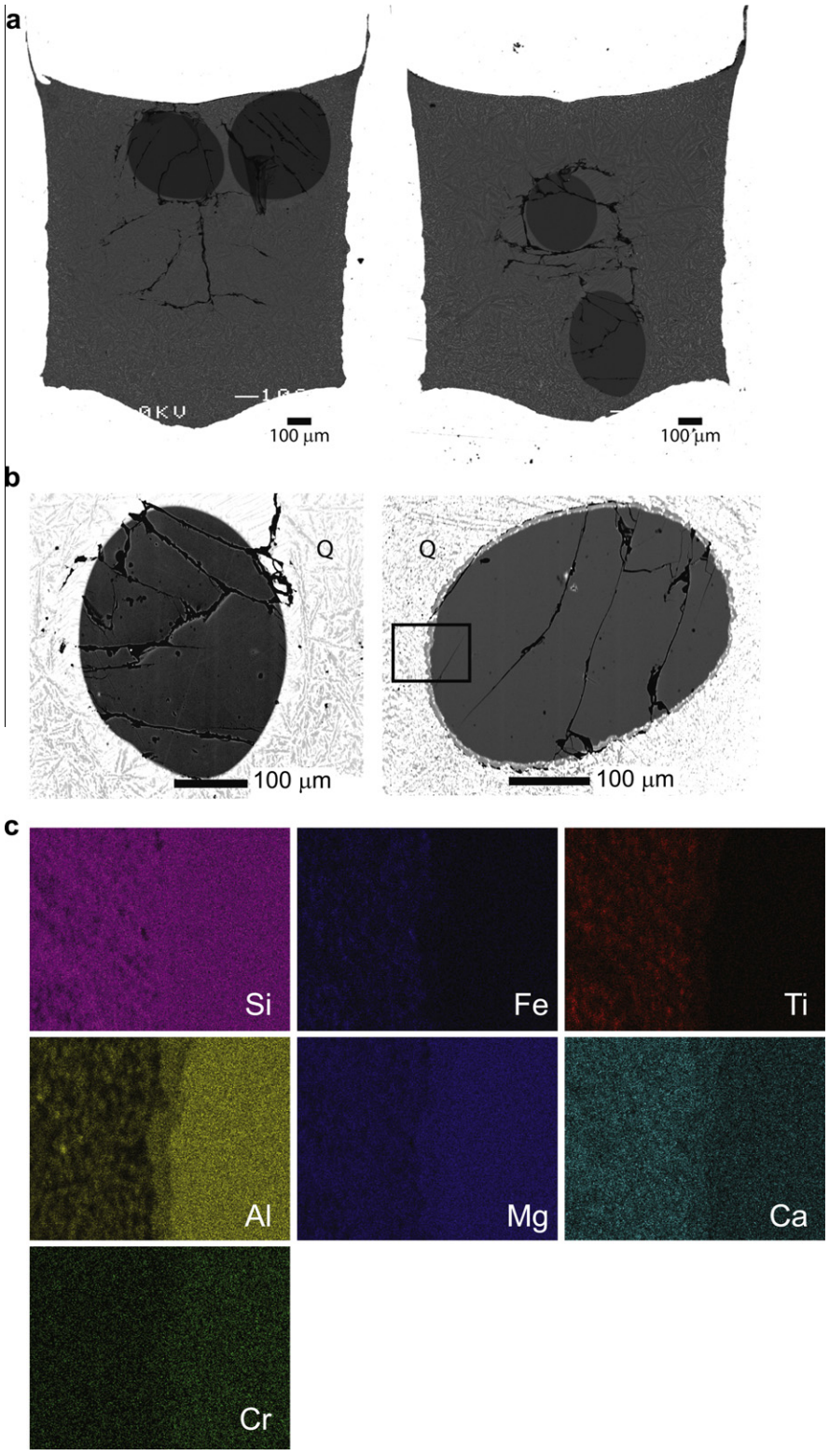

Fig. 1. (a) Representative back-scattered electron microprobe images of experiments using Fo_{100} spheres. Left image shows an experiment producing a float at $P = 1.7$ GPa, $T = 1744$ K and a sink result is shown in the right image (experiment at $P = 0.8$ GPa, $T = 1724$ K). (b) Representative back-scattered electron microprobe images of Fo_{90} (left) and garnet (right, $Py_{70}Al_{18}Gr_{12}$) spheres. Both spheres are surrounded by melt showing characteristic quench textures (Q). Note the absence of a reaction rim on the Fo_{90} sphere, and the ~10 μm wide reaction rim on the garnet sphere. (c) Element maps of the rectangular area (field of view ~90 μm width) in (b), showing the intermediate composition of the garnet reaction rim.

Table 3
Summary of experimental conditions and microprobe analyses. (a) Results for olivine (Fo_{100} and Fo_{90}) density marker experiments. (b) Results for experiments using garnet density markers of varying composition. Calculated liquid and ideal liquid densities at room pressure are derived from the data of Lange and Carmichael (1987). The liquid density is calculated from the experimental composition, whereas the ideal liquid density is calculated using the ideal Apollo 17 74,220 orange glass composition. For Cr_2O_3, MnO and MoO_2 no partial molar volumes are available. We estimated a partial molar volume of dissolved MoO_2 of 24 $cm^3\,mol^{-1}$ at 1773 K. The minor contributions of Cr_2O_3 and MnO are neglected for density determinations. Density marker sphere densities were calculated using Eqs. (1,2,3).

Sphere	Fo_{100}					
P (GPa)	0.5	0.8	1.0	1.3	1.7	2.0
T (K)	1724	1724	1727	1739	1744	1768
Result	Sink	Sink	NB	NB	Float	Float
(a)						
SiO_2	39.6(6)	40.2(12)	40.5(10)	38.5(12)	39.2(11)	39.6(18)
TiO_2	8.77(31)	8.33(69)	8.45(52)	8.92(49)	8.60(33)	8.47(89)
Al_2O_3	5.84(15)	6.37(99)	6.21(61)	6.20(82)	6.05(26)	6.15(83)
Cr_2O_3	0.53(17)	0.52(20)	0.41(25)	0.57(22)	0.51(17)	0.53(19)
FeO	21.3(3)	20.9(23)	20.4(11)	22.5(14)	21.1(16)	21.1(19)
MgO	15.0(6)	15.9(25)	16.3(13)	14.7(13)	16.1(14)	15.6(26)
MnO	0.28(2)	0.27(2)	0.28(2)	0.29(2)	0.28(2)	0.28(3)
CaO	7.32(26)	7.07(92)	7.03(51)	7.58(56)	7.26(49)	7.24(75)
Na_2O	0.36(2)	0.39(32)	0.26(19)	0.38(17)	0.23(15)	0.32(22)
MoO_2	1.00(30)	0.36(27)	0.60(45)	0.61(68)	0.99(85)	1.37(78)
Total	99.9(2)	100.2(8)	100.4(4)	100.2(6)	100.3(6)	100.7(6)
ρ_{liq}	2.97	2.95	2.95	2.98	2.97	2.96
$\rho_{ideal\ liq}$	2.99	2.99	2.99	2.98	2.98	2.97
ρ_{sphere}	3.07	3.08	3.09	3.09	3.11	3.11

Sphere	Fo_{90}			
P (GPa)	2.0	2.4	2.5	3.0
T (K)	1773	1794	1823	1853
Result	Sink	Sink	Sink	Float
SiO_2	41.7(18)	42.2(14)	39.9(10)	38.5(11)
TiO_2	8.33(96)	7.81(64)	8.48(76)	8.77(56)
Al_2O_3	5.91(26)	5.94(22)	5.86(20)	6.25(25)
Cr_2O_3	0.53(33)	0.67(22)	0.68(12)	0.67(8)
FeO	19.3(20)	19.0(18)	21.2(13)	22.4(10)
MgO	16.9(12)	17.1(12)	16.6(10)	15.0(8)
MnO	0.27(2)	0.26(2)	0.28(2)	0.29(2)
CaO	7.01(70)	7.00(83)	6.91(52)	7.64(23)
Na_2O	0.16(5)	0.17(6)	0.24(8)	0.33(10)
MoO_2	0.45(49)	0.76(36)	1.30(82)	0.66(41)
Total	100.6(4)	101.0(4)	101.3(3)	100.5(7)
ρ_{liq}	2.91	2.90	2.95	2.95
$\rho_{ideal\ liq}$	2.97	2.97	2.96	2.95
ρ_{sphere}	3.23	3.24	3.24	3.25

Sphere	$Py_{56}Al_{28}Gr_{16}$	$Py_{74}Al_{13}Gr_{13}$	$Py_{56}Al_{28}Gr_{16}$	$Py_{56}Al_{28}Gr_{16}$*	$Py_{70}Al_{18}Gr_{12}$	$Py_{77}Al_{14}Gr_{9}$	$Py_{70}Al_{18}Gr_{12}$	$Py_{67}Al_{20}Gr_{13}$ $Py_{74}Al_{14}Gr_{12}$	$Py_{70}Al_{20}Gr_{10}$	$Py_{74}Al_{14}Gr_{12}$
P (GPa)	5.5	6.0	6.5	6.5*	7.0	7.0	7.5	8.0	8.0	8.5
T (K)	2123	2123	2173	2173*	2193	2223	2223	2223	2223	2223
Result	Sink	NB	NB	NB	NB	NB	NB	NB	NB	Float/NB
(b)										
SiO_2	39.3(3)	38.7(29)	39.0(13)	39.1(5)	40.4(9)	40.0(14)	39.3(9)	39.3(14)	40.1(6)	39.2(11)
TiO_2	8.06(69)	8.77(175)	8.10(46)	7.90(3)	8.35(59)	8.36(70)	8.43(76)	8.34(111)	7.88(42)	8.57(65)
Al_2O_3	5.15(51)	6.25(81)	6.72(38)	6.60(76)	6.78(70)	6.73(130)	7.04(124)	6.73(181)	6.71(82)	6.55(76)
Cr_2O_3	0.68(1)	0.78(8)	0.78(2)	0.72(1)	0.72(5)	0.67(12)	0.66(9)	0.68(13)	0.84(8)	0.63(7)
FeO	21.8(8)	22.5(15)	20.9(8)	20.4(6)	19.8(8)	20.7(7)	19.8(9)	20.2(13)	20.4(4)	20.7(7)
MgO	16.0(1)	15.7(13)	15.9(4)	16.1(0)	15.5(3)	15.0(5)	15.5(4)	15.8(7)	16.2(2)	15.6(3)
MnO	0.27(3)	0.30(1)	0.29(2)	0.30(1)	0.30(2)	0.30(3)	0.29(3)	0.29(1)	0.31(3)	0.29(2)
CaO	7.58(28)	7.24(62)	7.37(30)	7.40(19)	7.39(22)	7.29(29)	7.47(23)	7.77(23)	7.62(1)	7.58(16)
Na_2O	0.30(2)	0.27(9)	0.29(1)	0.30(2)	0.33(3)	0.34(4)	0.33(4)	0.30(6)	0.27(3)	0.30(3)
MoO_2	2.19(147)	0.50(61)	2.08(102)	2.05(118)	0.90(106)	1.40(61)	1.17(61)	0.58(99)	1.03(75)	2.09(95)
Total	101.3(4)	101.0(3)	101.4(8)	100.8(5)	100.5(4)	100.8(7)	100.0(5)	100.0(7)	101.4(5)	101.5(5)
ρ_{liq}	2.89	2.88	2.86	2.85	2.82	2.83	2.82	2.82	2.82	2.84
$\rho_{ideal\ liq}$	2.87	2.87	2.86	2.86	2.85	2.85	2.85	2.85	2.85	2.85
ρ_{sphere}	3.73	3.63	3.74	3.74	3.68	3.65	3.69	3.72/3.68	3.72	3.69

Note: Experiment marked * used an experimental duration of 45 s.

Numbers in parentheses indicate one standard deviation (1σ) of replicate analyses in terms of last significant numbers: 39.3(3) should be read as 39.3 ± 0.3.

Table 4
Compositional analysis on used density markers (in wt%), *n* is the number of analysis. Table 3 shows in which experiment the spheres were used.

Olivine	*n*	SiO_2	TiO_2	Al_2O_3	Cr_2O_3	FeO	MnO	MgO	CaO	NiO	CoO	Total
Synthetic Fo_{100}	47	42.9(4)	0.01(1)	0.00(1)	ND	0.06(4)	0.00(1)	55.8(5)	0.00(0)	0.01(1)	0.35(2)	99.2(4)
San Carlos Fo_{90}	38	41.1(4)	0.02(1)	0.03(3)	0.03(1)	8.90(15)	0.11(1)	49.4(5)	0.09(1)	0.39(2)	ND	100.0(5)
Garnets		SiO_2	TiO_2	Al_2O_3	Cr_2O_3	FeO	MnO	MgO	CaO	MoO_2	Na_2O	Total
$Py_{56}Al_{28}Gr_{16}$	15	40.4(3)	0.06(2)	22.4(2)	0.17(2)	14.2(2)	0.37(1)	15.9(2)	6.13(5)	0.01(1)	0.01(1)	99.7(7)
$Py_{67}Al_{20}Gr_{13}$	1	42.6	1.71	18.6	3.13	10.4	0.31	20.1	5.40	0.00	0.03	102.2
$Py_{70}Al_{18}Gr_{12}$	21	41.9(6)	0.23(5)	21.3(3)	2.77(27)	8.09(97)	0.35(6)	20.9(11)	4.16(59)	0.01(1)	0.04(1)	99.8(10)
$Py_{70}Al_{20}Gr_{10}$	6	41.3(2)	0.14(2)	22.2(1)	1.11(7)	10.4(1)	0.42(2)	20.1(1)	4.16(1)	0.01(1)	0.02(1)	99.9(3)
$Py_{74}Al_{13}Gr_{13}$	6	41.5(2)	0.09(1)	19.4(1)	5.84(4)	6.80(5)	0.39(2)	21.6(1)	5.04(5)	0.01(2)	0.02(2)	100.6(3)
$Py_{74}Al_{14}Gr_{12}$	14	41.9(6)	0.32(2)	20.6(3)	3.15(5)	7.31(8)	0.29(2)	21.6(2)	4.95(11)	0.02(2)	0.04(2)	100.2(11)
$Py_{77}Al_{14}Gr_9$	11	42.2(7)	0.19(1)	21.2(3)	2.52(4)	7.19(7)	0.30(3)	21.9(3)	3.61(3)	0.01(1)	0.04(1)	99.2(10)

Numbers in parentheses indicate one standard deviation (1σ) of replicate analyses in terms of last significant numbers: 42.9(4) should be read as 42.9 ± 0.4. *n* indicates number of analyses.

high pressure, higher temperature experiments, which show average MoO_2 contents of 1.44 wt% with a 1σ of 0.67, compared to 0.81 wt% and 1σ of 0.34 for the low pressure, lower temperature experiments.

Experiments in which no up or down movement of spheres was observed were considered 'neutral buoyancy' when constrained by a sink and a float experiment at slightly lower and higher pressures, respectively. Neutral buoyancy results indicate that the densities of the spheres are very close or equal to the density of the molten glass at the experimental *P–T*. There is ambiguity in experiments where the spheres did not move and when unconstrained by a sink and/or float experiments at slightly lower and higher pressures, since we cannot prove that the spheres remained fixed because of other factors such as adhesion to the capsule wall or low sinking/rising rates.

In the experiments using olivine markers we obtained three floats, five sinks, and two neutral buoyancies. The resulting density brackets for the A17 orange glass composition at near liquidus temperatures for lunar interior pressure conditions are given in Table 3a and shown by the symbols in Fig. 2. The two neutral buoyancies using the Fo_{100} spheres were confirmed by sinks and floats at slightly lower and higher pressures (Table 3a). They indicate molten orange glass densities are 3.09 ± 0.06 g cm^{-3} at $P =$ 1.0 GPa, $T = 1727$ K, and 3.09 ± 0.02 g cm^{-3} at $P =$ 1.3 GPa, $T = 1739$ K. A third measurement, bracketed by a sink and float experimental result, but not including a neutral buoyancy experiment, indicates a density of 3.25 ± 0.02 g cm^{-3} at $P \sim 2.8$ GPa, $T \sim 1838$ K (Fig. 2).

For the experiments using the pyrope-rich garnet density markers we found one sink and one float close to neutral buoyancy (Fig. 3a). In the other seven garnet-bearing experiments no sphere movement was observed, potentially reflecting neutral buoyancy but not bracketed by sinks and floats at near *P–T* conditions. These neutrally buoyant experiments, with garnet compositions ranging from $Py_{56}Al_{28}Gr_{16}$ to $Py_{77}Al_{14}Gr_9$ (Tables 3b and 4) were observed in the *P–T* range between 6.0 and 8.0 GPa and 2173–2223 K. In the experiment where a denser sphere was placed at the top of the charge and a less dense sphere at the bottom (Table 3b), both spheres remained at their original positions. This ambiguous result can be explained in two ways. Either the experiment did not yield true neutral buoyancy, with one or both of the spheres adhering to the capsule wall, or falling/rising velocities were too low to lead to discernible movement, or the liquid was very near neutral buoyancy for one or both of the spheres but the duration of the experiment was too short for stokes

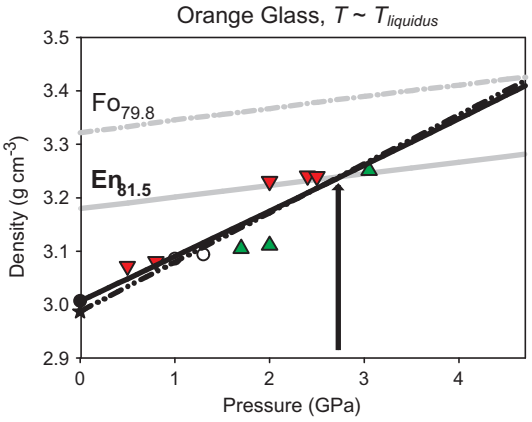

Fig. 2. Density vs. pressure diagram summarising the sink/float experiments at lunar pressures (data taken from Table 4a) at $T \sim T_{liquidus}$. For all experiments olivine density markers were used. Downward pointing triangles indicate sinks, upward pointing triangles floats and open circles represent experiments in which no sphere movement was observed. Symbols are slightly larger than the error bars, ± 0.02 g cm^{-3}. Black curve is the interpreted density curve, using the calculated 1 bar density point (Lange and Carmichael, 1987) of 3.01 g cm^{-3} (black dot) and the experimental constraints. Dashed dotted curve is the interpreted density curve, using the calculated 1 bar density point (Ghiorso and Kress, 2004) of 2.99 g cm^{-3} (black star) and the experimental constraints. $Fo_{79.8}$ and $En_{81.5}$ lines indicate density variations for equilibrium compositions of olivine and orthopyroxene, derived using mineral compositions from Krawczynski and Grove (2008). Arrow indicates density crossovers with orthopyroxene. Density crossover with olivine falls just outside the lunar pressure range. (For interpretation of the references to colour in this figure legend, the reader is referred to the web version of this article.)

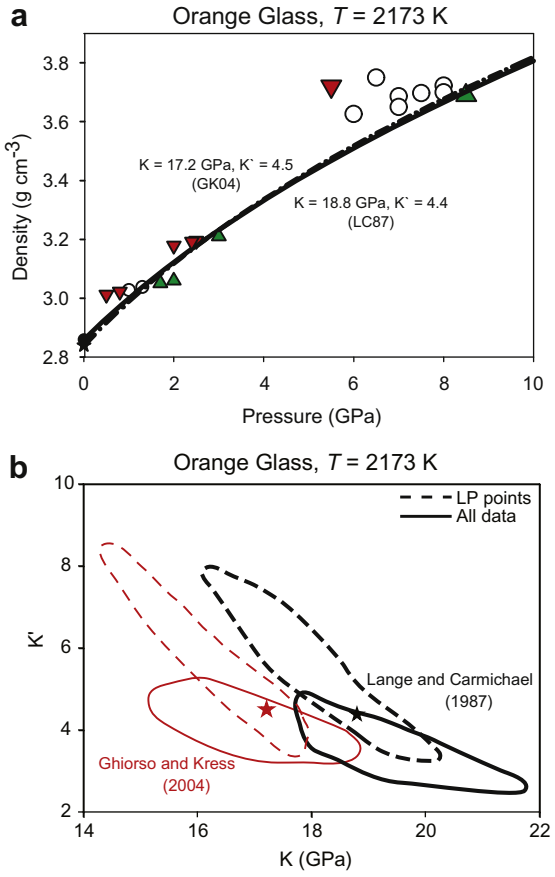

Fig. 3. (a) Summary of all experiments on synthetic molten Apollo 17 orange glass and best-fit density curves at 2173 K. Symbols are as in Fig. 2. Olivine and garnet-bearing experiment symbols are roughly equal in size to the error bars, of (0.02 g cm^{-3} and ±0.04 g cm^{-3}, respectively. The two density lines were evaluated using the 1 bar density of 2.86 and 2.84 g cm^{-3} calculated using Lange and Carmichael (1987, LC87) and Ghiorso and Kress (2004, GK04), respectively. Solid line starting with black dot LC87 and dashed dotted line starting with black star GK04. (b) Range of acceptable Birch–Murnaghan values for the isothermal bulk modulus at 2173 K, $K_{2173\ K}$ and its pressure derivative K' for molten Apollo 17 orange glass, using the 1 bar density values calculated using Lange and Carmichael (1987) and Ghiorso and Kress (2004). The solid envelopes consider all experimental results, whereas dashed fields are solutions considering the lower pressure experiments with olivine density markers only. The stars show best-fit solutions to the low pressure data plotted as curves in (a). (For interpretation of the references to colour in this figure legend, the reader is referred to the web version of this article.)

settling to cause movement. In the experiment with a duration of 45 s no sphere movement was observed either (Table 3b). Longer run durations are not practical due to increased Mo contamination and enhanced sphere reaction with the melt (e.g. Circone and Agee, 1996). Although we could not pinpoint the reason for the large number of neutral buoyancies in our MA experiments, we conclude that tighter brackets on molten orange glass density are difficult to obtain with our current experimental setup.

4. DISCUSSION

4.1. Density crossovers in the lunar mantle

Our experiments provide tight bounds on the density of molten A17 orange glass by the sink, float and neutral buoyancies of the olivine-bearing experiments, which were all performed within the lunar P–T range. To calculate the density profile of molten A17 in the lunar P range we combined our low P results with a 1 bar density anchor point of 3.01 g cm^{-3}, calculated using the compositional parameters of Lange and Carmichael (1987) at the estimated $T_{liquidus}$ of 1645 K (solid line, Fig. 2). Contributions of the minor elements Cr_2O_3 and MnO were neglected since no compositional parameters are available for these oxides. To assess the sensitivity of our results to the chosen 1 bar density anchor point, Fig. 2 also shows the density curve using the calculated 1 bar density obtained with the compositional parameters of Ghiorso and Kress (2004) (2.99 g cm^{-3}, dash dotted line).

To determine the conditions at which density crossovers occur for the orange glass composition, the densities of the equilibrium coexisting olivines and pyroxenes have to be calculated (Delano, 1990). Mineral densities depend mainly on their magnesium numbers, which may be related to liquid composition through application of crystal (s)–liquid (l) distribution coefficients (Roeder and Emslie, 1970):

$$K_D = \left(\frac{X_{FeO}}{X_{MgO}}\right)^s \left(\frac{X_{MgO}}{X_{FeO}}\right)^l \quad (4)$$

In order to calculate the importance of potential density crossovers with molten A17 orange glass we use average K_D values for olivine and orthopyroxene from the orange glass composition phase equilibrium experiments of Krawczynski and Grove (2008). The average K_D values are 0.294 for olivine and 0.263 for orthopyroxene, resulting in equilibrium compositions of $Fo_{79.8}$ and $En_{81.5}$. Resulting crossover pressures between molten orange glass and orthopyroxene are close to ~2.8 GPa (Fig. 2), equivalent to a depth of ~600 km in the lunar mantle, at a density of ~3.25 g cm^{-3}. This crossover pressure is not sensitive to the choice of 1 bar density anchor point. At $P < 2.8$ GPa, molten orange glass is thus less dense than its equilibrium orthopyroxenes. Krawczynski and Grove (2008) showed that the multiple saturation point (msp) for the A17 orange glass composition lies at pressures between 2.5 and 3.1 GPa depending on the oxygen fugacity. At the oxygen fugacity estimated for natural orange glass (Sato, 1979; Weitz et al., 1997; Nicholis and Rutherford, 2009), the MSP is approximately 2.8–2.9 GPa. As such the buoyancy of molten orange glass does not pose a constraint on its extraction.

Density crossovers for the molten A17 orange glass with olivine are just outside the P range of the Moon, indicating that molten orange glass is less dense than its equilibrium olivines. A density crossover beyond the lunar pressure range was also observed for the green glass composition (Smith and Agee, 1997). Molten black glass remains the only investigated lunar liquid (Circone and Agee, 1996)

for which a density crossover with olivine at lunar pressures is possible.

4.2. Compressibility of molten lunar glasses

Fig. 2 shows the density of the molten orange glass along the liquidus at lunar pressure conditions. The neutral buoyancy results at 1.0 and 1.3 GPa suggest an initial density increase with pressure along the liquidus of ~0.07–0.08 g cm^{-3} GPa^{-1}, assuming a 1 bar density value calculated using the model of Lange and Carmichael (1987). When assuming the 1 bar density value calculated via the model of Ghiorso and Kress (2004) we find a slightly larger slope ~0.08–0.10 g cm^{-3} GPa^{-1}. Between the 1.3 GPa neutral buoyancy point and the ~2.8 GPa anchor point the density slope is comparable to the initial slope at ~0.10 g cm^{-3} GPa^{-1} when using the model of Ghiorso and Kress (2004).

The results of the MA experiments using the pyrope-rich garnet spheres, beyond the lunar P–T range, have larger errors with an array of experiments in which no sphere movement was observed and significantly wider sink/float bounds. As a result, there is a wide array of acceptable Birch–Murnaghan (BM) EOS parameter combinations that is consistent with our complete data set (both high and low pressure experiments). For a temperature of 2173 K, Fig. 3b shows the acceptable combinations of values for the isothermal bulk modulus $K_{2173\ K}$ and its pressure derivative K'. Since the high pressure garnet data show a scatter of experiments in which no sphere movement was observed (Fig. 3a), we evaluated the molten A17 orange glass EOS with and without incorporating the results of these higher pressure points. When only incorporating the low pressure data points and anchoring the fits using the 1 bar calculated density value of Lange and Carmichael (1987), $\rho_{0,2173\ K} = 2.86$ g cm^{-3}, we obtain an array of solutions with $K_{2173\ K}$ between 16.1 and 20.3 GPa and K' between 3.6 and 8.0. Best-fit values are 18.8 GPa and 4.4, respectively (solid black line in Fig. 3a). Anchoring the fits using the 1 bar calculated density value of Ghiorso and Kress (2004), $\rho_{0,2173\ K} = 2.84$ g cm^{-3}, leads to an array of solutions with $K_{2173\ K}$ between 14.4 and 18.0 GPa and K' between 3.7 and 8.7, with best-fit values 17.2 GPa and 4.5, respectively (dashed dotted line in Fig. 3a).

When incorporating the high pressure data points, the array of acceptable K–K' combinations shift towards slightly higher K and lower K' values (Fig. 3b). The shift in position and size of the envelope of acceptable solutions resulting from incorporating these higher pressure experiments illustrates the importance of such experiments for constraining liquid EOS parameters. The relatively large range of acceptable solutions even when incorporating all results shows that additional experiments at higher pressure with narrow sink/float brackets are required to provide tighter bounds on the molten A17 orange glass EOS parameters. The uncertainty in the 1 bar density anchor point illustrates the importance of this value too.

Finally, in Fig. 4 we compare the densities of molten orange and black glass on isothermal compression curves. Unfortunately we could not add a molten green glass curve

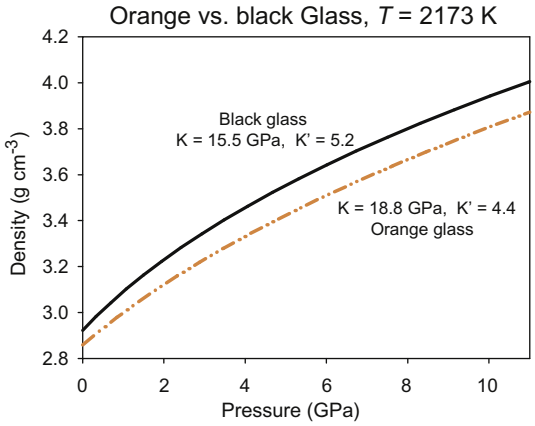

Fig. 4. Comparison of density curves for molten orange (orange dashed dotted line) and molten black glass (black solid line). For both density curves the 1 bar density values calculated from Lange and Carmichael (1987) were used. (For interpretation of the references in colour in this figure legend, the reader is referred to the web version of this article.)

for comparison since no temperature-dependent K and K' values are available for this composition (Smith and Agee, 1997). Clearly these curves are not parallel, indicating different compression behaviour for the two compositions. The observed variations in compressibility between the molten lunar glasses are likely related to their different TiO_2 contents (e.g. Webb and Dingwell, 1994), which is the biggest compositional difference between orange and black glass.

4.3. The effect of titanium on melt density and compressibility

As illustrated in the preceding section, small variations in the position of the 1 bar density anchor point can lead to significant differences in the predicted variations in density with P and T. The 1 bar density difference between the models of Lange and Carmichael (1987) and Ghiorso and Kress (2004), neglecting the minor contributions of both Cr_2O_3 and MnO, is 0.6%, at the estimated liquidus T of 1645 K. This small initial density difference results in a difference of 8.5% in the best fit value of the isothermal bulk modulus, and of 2.3% in values of its pressure derivative K'.

Uncertainties in the partial molar volume of TiO_2, needed to calculate the 1 bar density, lie at the heart of this issue. These uncertainties are caused in part by the fact that tetravalent titanium shows variable coordination with oxygen in silicate melts as well as hydrous fluids (Farges et al., 1996; Romano et al., 2000; Liu and Lange, 2001; Guillot and Sator, 2007; Van Sijl et al., 2010). In the case of silicate melts, this has an important effect on the melt properties. For example, the asymmetric geometry of 5-fold coordinated Ti promotes different topological rearrangements in the melt, leading to enhanced compressibility of TiO_2. TiO_2 is found to be twice as compressible as Na_2O and SiO_2 in liquids when Ti is in 5-fold coordination, whereas its compressibility is nearly identical to those of Na_2O and SiO_2 when Ti is entirely in 4-fold coordination (Liu et al., 2007). Since the density of silicate melts is largely

determined by the geometrical packing and coordination of its network forming ions, the capacity of Ti^{4+} to shift coordination will strongly affect the one-bar density and one-bar compressibility (Liu and Lange, 2001; Liu et al., 2007).

We do not know the coordination numbers of titanium in our samples, nor is this information available for the natural picritic lunar magmas. As a result it is not possible to provide an answer to the question of what the 1 bar density value of molten orange glass is. More accurate density estimates of lunar magmas require measurements of the coordination state of titanium.

5. CONCLUSIONS

The density of synthetic molten Apollo 17 orange glass has been investigated up to a pressure of 8.5 GPa. Density determinations have been performed using the sink/float technique and olivine and garnet density markers. The resulting density crossover of this composition with orthopyroxene at ~2.8 GPa is higher than the orange glass composition multiple saturation point. As such the buoyancy of orange molten does not hinder its extraction.

The array of acceptable Birch–Murnaghan (BM) EOS parameter combinations that is consistent with our data is $K_{2173\ K}$ 16.1–20.3 and K' 3.6–8.0, best-fit values are 18.8 GPa and 4.4, respectively, when assuming the 1 bar density value of Lange and Carmichael (1987). However, when using the data of Ghiorso and Kress (2004) to derive the 1 bar density value we obtain $K_{2173\ K}$ 14.4–18.0 and K' 3.7–8.7, with best-fit values of 17.2 GPa and 4.5, respectively.

Additional experiments, at high pressure, on orange glass composition with narrow sink/float brackets at higher pressures (~8–12 GPa), are needed to provide tighter bounds on K_T and K'. Besides additional experiments to refine the range of possible EOS parameters it is essential to have a correct value for the 1 bar density value, requiring knowledge of the coordination state of titanium.

ACKNOWLEDGMENTS

We thank Mike Krawczynski (MIT) for providing the Apollo 17 orange glass composition starting material. We also thank Wim Lustenhouwer (VU) and Mike Spilde (IOM) for their assistance during microprobe analyses and Jellie de Vries (Utrecht University and VU) and Michel Jacobs (Clausthal University) for their help with EOS calculations. We thank Dave Draper and Steve Elardo for their help in the lab. Bob Luth, Rebecca Lange, Mike Toplis and one anonymous reviewer are acknowledged for their insightful comments on an earlier version of this manuscript. This work was supported by a VU University Ph.D. student grant to MvKP and a European Science Foundation EURYI award to WvW.

REFERENCES

Agee C. B. (1998) Crystal–liquid density inversions in terrestrial and lunar magmas. *Phys. Earth Planet. Inter.* **107**, 63–74.

Agee C. B. (2008) Static compression of hydrous silicate melt and the effect of water on planetary differentiation. *Earth Planet. Sci. Lett.* **265**, 641–654.

Agee C. B. and Walker D. (1988) Static compression and olivine flotation in ultrabasic silicate liquid. *J. Geophys. Res. Solid Earth Planets* **93**, 3437–3449.

Agee C. B. and Walker D. (1993) Olivine flotation in mantle melt. *Earth Planet. Sci. Lett.* **114**, 315–324.

Angel R. J. (2000) Equations of state. *High-Temp. High-Press. Cryst. Chem.* **41**, 35–59.

Birch F. (1947) Finite elastic strain of cubic crystals. *Phys. Rev.* **71**, 809–824.

Bond W. L. (1951) Making small spheres. *Rev. Sci. Instrum.* **22**, 344–345.

Chopelas A. (2006) Modeling the thermodynamic parameters of six endmember garnets at ambient and high pressures from vibrational data. *Phys. Chem. Miner.* **33**, 363–376.

Circone S. and Agee C. B. (1995) Effect of pressure on cation partitioning between immiscible liquids in the system TiO_2–SiO_2. *Geochim. Cosmochim. Acta* **59**, 895–907.

Circone S. and Agee C. B. (1996) Compressibility of molten high-Ti mare glass: evidence for crystal–liquid density inversions in the lunar mantle. *Geochim. Cosmochim. Acta* **60**, 2709–2720.

Conrad P. G., Zha C. S., Mao H. K. and Hemley R. J. (1999) The high-pressure, single-crystal elasticity of pyrope, grossular, and andradite. *Am. Miner.* **84**, 374–383.

Delano J. W. (1986) Pristine lunar glasses – criteria, data, and implications. *J. Geophys. Res. Solid Earth Planets* **91**, D201–D213.

Delano J. W. (1990) Buoyancy-driven melt segregation in the earths moon. 1: Numerical results. *Proc. Lunar Planet. Sci. Conf.* **20**, 3–12.

Elkins-Tanton L. T., Chatterjee N. and Grove T. L. (2003a) Magmatic processes that produced lunar fire fountains. *Geophys. Res. Lett.* **30**(10), 1513.

Elkins-Tanton L. T., Chatterjee N. and Grove T. L. (2003b) Experimental and petrological constraints on lunar differentiation from the Apollo 15 green picritic glasses. *Meteorit. Planet. Sci.* **38**(4), 515–527.

Farges F., Brown G. E. and Rehr J. J. (1996) Coordination chemistry of Ti(IV) in silicate glasses and melts. 1: XAFS study of titanium coordination in oxide model compounds. *Geochim. Cosmochim. Acta* **60**, 3023–3038.

Geiger C. A. (1999) Thermodynamics of $(Fe^{2+}, Mn^{2+}, Mg, Ca)_3$–$Al_2Si_3O_{12}$ garnet: a review and analysis. *Mineral. Petrol.* **66**, 271–299.

Ghiorso M. S. and Kress V. C. (2004) An equation of state for silicate melts. II: Calibration of volumetric properties at 10^5 Pa. *Am. J. Sci.* **304**, 679–751.

Graham E. K., Schwab J. A., Sopkin S. M. and Takei H. (1988) The pressure and temperature-dependence of the elastic properties of single-crystal fayalite Fe_2SiO_4. *Phys. Chem. Miner.* **16**, 186–198.

Grove T. L. and Krawczynski M. J. (2009) Lunar mare volcanism: where did the magmas come from? *Elements* **5**, 29–34.

Guillot B. and Sator N. (2007) A computer simulation study of natural silicate melts. Part I: low pressure properties. *Geochim. Cosmochim. Acta* **71**, 1249–1265.

Hazen R. M. (1977) Effects of temperature and pressure on crystal-structure of ferromagnesian olivine. *Am. Miner.* **62**, 286–295.

Hugh-Jones D. (1997) Thermal expansion of $MgSiO_3$ and $FeSiO_3$ ortho- and clinopyroxenes. *Am. Miner.* **82**, 689–696.

Hugh-Jones D. A. and Angel R. J. (1994) A compressional study of $MgSiO_3$ orthoenstatite up to 8.5-GPa. *Am. Miner.* **79**, 405–410.

Hugh-Jones D. A. and Angel R. J. (1997) Effect of Ca^{2+} and Fe^{2+} on the equation of state of $MgSiO_3$ orthopyroxene. *J. Geophys. Res. Solid Earth* **102**, 12333–12340.

Hushur A., Manghani M. H., Smyth J. R., Nestola F. and Frost D. J. (2009) Crystal chemistry of hydrous forsterite and its vibrational properties up to 41 GPa. *Am. Miner.* **94**, 751–760.

Isaak D. G., Graham E. K., Bass J. D. and Wang H. (1993) The elastic properties of single-crystal fayalite as determined by dynamical measurement techniques. *Pure Appl. Geophys.* **141**, 393–414.

Jacobs M. H. G. and de Jong B. (2007) Placing constraints on phase equilibria and thermophysical properties in the system $MgO–SiO_2$ by a thermodynamically consistent vibrational method. *Geochim. Cosmochim. Acta* **71**, 3630–3655.

Knoche R. and Luth R. W. (1996) Density measurements on melts at high pressure using the sink/float method: limitations and possibilities. *Chem. Geol.* **128**, 229–243.

Krawczynski M. J. and Grove T. L. (2008) Experimental investigations of f_{O_2} effects on Apollo 17 orange glass phase equilibria. *Lunar Planet. Sci. Conf.* **39**, 1231.

Lange R. A. and Carmichael I. S. E. (1987) Density of $Na_2O–K_2O–CaO–MgO–FeO–Fe_2O_3–Al_2O_3–TiO_2–SiO_2$ liquids: new measurements and derived partial molar properties. *Geochim. Cosmochim. Acta* **51**, 2931–2946.

Lavrentiev M. Y., van Westrenen W., Allan N. L., Freeman C. L. and Purton J. A. (2006) Simulation of thermodynamic mixing properties of garnet solid solutions at high temperatures and pressures. *Chem. Geol.* **225**, 336–346.

Liu Q. and Lange R. A. (2001) The partial molar volume and thermal expansivity of TiO_2, in alkali silicate melts: systematic variation with Ti coordination. *Geochim. Cosmochim. Acta* **65**, 2379–2393.

Liu Q., Lange R. A. and Ai Y. H. (2007) Acoustic velocity measurements on $Na_2O–TiO_2–SiO_2$ liquids: evidence for a highly compressible TiO_2 component related to five-coordinated Ti. *Geochim. Cosmochim. Acta* **71**, 4314–4326.

Liu W. and Li B. S. (2006) Thermal equation of state of $(Mg_{0.9}Fe_{0.1})_2SiO_4$ olivine. *Phys. Earth Planet. Inter.* **157**, 188–195.

Nicholis M. G. and Rutherford M. J. (2009) Graphite oxidation in the Apollo 17 orange glass magma: implications for the generation of a lunar volcanic phase. *Geochim. Cosmochim. Acta* **73**, 5905–5917.

O'Neill H. St. C. (1986) $Mo–MoO_2$ (MOM) oxygen buffer and the free energy of formation of MoO_2. *Am. Miner.* **71**, 1007–1010.

Roeder P. L. and Emslie R. F. (1970) Olivine–liquid equilibrium. *Contrib. Mineral. Petrol.* **29**, 275–289.

Romano C., Paris E., Poe B. T., Giuli G., Dingwell D. B. and Mottana A. (2000) Effect of aluminum on Ti-coordination in silicate glasses: a XANES study. *Am. Miner.* **85**, 108–117.

Sato M. (1979) The driving mechanism of lunar pyroclastic eruptions inferred from the oxygen fugacity behavior of Apollo 17 orange glass. In *Lunar and Planetary Science Conference Proceedings* (ed. N. W. Hinners). pp. 311–325.

Shearer C. K., Hess P. C., Wieczorek M. A., Pritchard M. E., Parmentier E. M., Borg L. E., Longhi J., Elkins-Tanton L. T., Neal C. R., Antonenko I., Canup R. M., Halliday A. N., Grove T. L., Hager B. H., Lee D. C. and Wiechert U. (2006) Thermal and magmatic evolution of the moon. *Rev. Mineral. Geochem.* **60**, 365–518.

Skinner B. J. (1966) Thermal expansion. In *Handbook of Physical Constants* (ed. S. P. Clark).

Smith J. R. and Agee C. B. (1997) Compressibility of molten ''green glass'' and crystal–liquid density crossovers in low-Ti lunar magma. *Geochim. Cosmochim. Acta* **61**, 2139–2145.

Smyth J. R. (1975) High temperature crystal-chemistry of fayalite. *Am. Miner.* **60**, 1092–1097.

Sumino Y. and Anderson O. L. (1984) Elastic constants of minerals. In *CRC Handbook of the Physical Properties of Rocks* (ed. S. Carmichael). CRC Press, Boca, Raton, FL.

Suzuki A. and Ohtani E. (2003) Density of peridotite melts at high pressure. *Phys. Chem. Miner.* **30**, 449–456.

Suzuki A., Ohtani E. and Kato T. (1995) Flotation of diamond in mantle melt at high-pressure. *Science* **269**, 216–218.

Suzuki I. (1975) Thermal expansion of periclase and olivine, and their anharmonic properties. *J. Phys. Earth* **23**, 145–159.

Suzuki I., Seya K., Takei H. and Sumino Y. (1981) Thermal-expansion of fayalite, Fe_2SiO_4. *Phys. Chem. Miner.* **7**, 60–63.

van Sijl S., Allan N. L., Davies G. R. and van Westrenen W. (2010) Titanium in subduction zone fluids: first insights from ab initio metadynamics simulations. *Geochim. Cosmochim. Acta* **74**, 2797–2810.

van Westrenen W., Van Orman J. A., Watson H., Fei Y. and Watson E. B. (2003) Assessment of temperature gradients in multianvil assemblies using spinel layer growth kinetics. *Geochem. Geophys. Geosyst.* 4(1), doi: 10.1029/2002GC000474.

Wagner T. P. and Grove T. L. (1997) Experimental constraints on the origin of lunar high-Ti ultramafic glasses. *Geochim. Cosmochim. Acta* **61**, 1315–1327.

Watson E. B., Wark D. A., Price J. D. and Van Orman J. A. (2002) Mapping the thermal structure of solid-media pressure assemblies. *Contrib. Mineral. Petrol.* **142**, 640–652.

Webb S. L. and Dingwell D. B. (1994) Compressibility of titanosilicate melts. *Contrib. Mineral. Petrol.* **118**, 157–168.

Weitz C. M., Rutherford M. J. and Head, III, J. W. (1997) Oxidation states and ascent history of the Apollo 17 volcanic beads as inferred from metal–glass equilibria. *Geochim. Cosmochim. Acta* **61**, 2765–2775.

Zhang L., Ahsbahs H., Kutoglu A. and Geiger C. A. (1999) Single-crystal hydrostatic compression of synthetic pyrope, almandine, spessartine, grossular and andradite garnets at high pressures. *Phys. Chem. Miner.* **27**, 52–58.

Associate editor: Michael Toplis